Predicting Early EVA Degradation in Photovoltaic Modules From Short Circuit Current Measurements

Hussain A. Al Mahdi, Paul G. Leahy, and Alan P. Morrison, *Senior Member, IEEE*

***Abstract*—One of the common failures in photovoltaic modules is the degradation of the ethylene-vinyl acetate (EVA) encapsulant due to prolonged ultraviolet exposure and other environmental stress factors, such as temperature and humidity. Experimental studies have shown that significant reduction in the optical transmission due to EVA degradation leads to loss in the available power by more than 50%. In this article, a novel approach to predict the early degradation of EVA encapsulant is proposed by correlating EVA degradation with short-circuit current (I_{SC}). An electrical circuit simulator, simulation program with integrated circuit emphasis (SPICE), is used to evaluate the short-circuit current obtained under varying optical transmission caused by EVA discoloration. The simulation follows three steps: simulation of the transmitted solar spectrum; simulation of the spectral short-circuit current density; and simulation of the current-voltage (*I–V*) curve to obtain short-circuit current (I_{SC}), maximum power output (P_{max}), open-circuit voltage (V_{OC}) and fill factor. Results show that the reduction in short-circuit current due to EVA degradation differs from the reductions expected due to a spectrally-uniform reduction of intensity of the solar irradiance. Both types of variation are linear, however, the slope due to EVA degradation is larger than the slope obtained for normal intensity variations in the solar irradiance. This model, when applied in conjunction with solar irradiance measurements, can predict early onset of EVA encapsulant failure, thereby enabling preventative measures to be taken.**

***Index Terms*—Encapsulant transmittance, ethylene-vinyl acetate (EVA) degradation, photovoltaic (PV) module deterioration, PV module reliability, short-circuit current measurement, SPICE simulation.**

I. Introduction

THE SOLAR spectrum consists of light having wavelengths of varying intensity. The solar spectrum is typically divided into three wavelength regions: ultraviolet (UV); visible; and infrared; some of which can be absorbed by crystalline silicon solar cells and converted into electrical energy. Typically, a silicon solar cell absorbs light within the wavelength range of 0.310 to 1.18 μm. According to [1], the spectral response for monocrystalline solar cells is in the range of 0.35 to 1.1 μm. Absorbed light that is not converted into captured charge is dissipated as heat, leading to an increase in the operating temperature of the solar cell. In general, solar cells are packaged into modules by placing a polymer layer, called the encapsulant, between the solar cells and the tempered glass to increase light absorption and reduce light reflection [2].

Several different materials have been used as encapsulants for photovoltaic (PV) modules including thermoplastic polyurethane and polydimethylsiloxane [3]–[5]. The latter is superior to other encapsulants when it comes to immunity against environmental stress and UV radiation. For this reason, it was used in the early development of PV encapsulation [6]. Modern alternative encapsulants include Ionomers (DuPont) that are claimed to have up to 25 times the effectiveness of EVA in preventing potential induced degradation and polyolefins (Dow chemicals) that offer claims of superior electrical resistance and moisture rejection than either EVA or ionomers [7], [8]. However, a tradeoff between cost and immunity from environmental stress has favoured ethylene vinyl acetate (EVA), which is why EVA is currently used in almost 80% of all PV modules [9]. Vinyl acetate represents up to 33% of the encapsulant composition while the remaining percentage is a mixture of ethylene, antioxidants and curing materials such as peroxide [10].

This article reviews reported encapsulant degradation from literature studies in Section II. SPICE is used to model the influence of EVA degradation on the performance of solar cells using experimental results from Pern *et al*. [11]. The SPICE model and its use is explained in more detail in Section III. A comparison between the short-circuit current density (J_{SC}) resulting from reduced transmission through degraded EVA and the corresponding J_{SC} resulting from the equivalent absorbed power density from the solar spectrum is demonstrated in Section IV. The results show that the differences in the slope of measured short-circuit current density can be used as an indicator of early onset of degradation of the EVA. These key results are introduced and discussed in Section V.

II. Encapsulant Degradation

A. Review of Encapsulant Degradation

Degradation of the encapsulant leads to poor optical performance in the PV module, leading to poor energy efficiency due to reduced light absorption and increased reflection [12]. One of the major causes of encapsulant degradation is ultraviolet radiation even though it represents less than 3.5% of the solar spectrum

Manuscript received March 10, 2021; revised May 12, 2021; accepted May 27, 2021. The work of Hussain Al Mahdi was supported by the Saudi Ministry of Education, under Grant IR18112. *(Corresponding author: Alan P. Morrison.)*

Hussain A. Al Mahdi and Alan P. Morrison are with the Department of Electrical and Electronic Engineering, School of Engineering, University College Cork, T12K8AF Cork, Ireland (e-mail: 118225936@umail.ucc.ie; a.morrison@ucc.ie).

Paul G. Leahy is with the Department of Energy Engineering, School of Engineering, University College Cork, T12K8AF Cork, Ireland (e-mail: paul.leahy@ucc.ie).

Color versions of one or more figures in this article are available at https://doi.org/10.1109/JPHOTOV.2021.3086455.

Digital Object Identifier 10.1109/JPHOTOV.2021.3086455

[13], [14]. Given its shorter wavelength, UV light has increased energy that degrades the encapsulant over time, typically by breaking down the polymeric bonds [15].

The ultraviolet spectrum is categorized into three regions: UV-A, UV-B, and UV-C. As PV panels are never naturally exposed to UV-C it is UV-B that is considered the most harmful in triggering the degradation process in EVA encapsulation [16], [17]. In order to reduce this effect, the PV protective glass is sometimes doped with cerium additive [18]. However, in a lab study conducted by King *et al.* [19], the use of cerium additive was found to cause a 2% reduction of the optical transmission in the long run. Moreover, Kempe *et al*. [20] investigated the effect of cerium removal from the protective glass and found that excluding cerium results in a gain of up to 1.8% in optical transmittance [18].This motivates some manufacturers to persevere without adding cerium. In contrast, its exclusion is considered a risk factor that leads to a threefold increase in the rate of encapsulant delamination [20]. Therefore, when it comes to the protective glass, it was concluded by Kempe *et al.* [20], that the exclusion of cerium has no benefit on electrical performance and if omitted, an antireflective coating must be added to the glass to block the UV spectrum below 350 nm.

However, even with the UV-blocking glass, if the UV irradiance is combined with temperature, the presence of additives, or other stress factors, it leads to deterioration of the EVA encapsulant [21]. As a result, a chemical reaction is triggered that produces acetic acid and aldehyde, altering the EVA color progressively from clear to light yellow, then yellow, yellow-brown, brown, and ultimately dark brown in critical cases [21].

An experiment conducted by Miller *et al*. [4], demonstrates the effect of UV exposure along with two other stress factors: humidity and temperature, on five different types of encapsulant. Results showed that the rate of degradation increases when encapsulants experience a combination of lower humidity and higher temperature. This leads to a greater discoloration of the encapsulant. A similar study by Arularasu [22], also investigated the effect of these two stress factors along with UV radiation on encapsulant degradation, with similar conclusions.

A term known as the "yellowness index" was introduced to quantify the discoloration effect. According to the International Standards Organization [23], the yellowness index is defined as a shift in polymer color toward yellow. However, in Oliveira *et al*. [24], it was found that even if the PV encapsulant color has not yet shifted to yellowness i.e., did not affect the yellowing index, it cannot be determined with certainty that degradation is not present. This uncertainty has motivated researchers, for instance [18], [25], [26], to investigate the starting point of the encapsulant degradation process.

While it was claimed by Ferrara and Philipp [27], that there is no clear relationship between the change in the encapsulant's color and electrical performance of the solar cell, it was experimentally proven by Rosillo and Alonso-Garcia [28], that the maximum power output ($P_{\max}$) is reduced when the yellowness index increases. This is in agreement with Pern *et al*. [11], who conducted an experiment in 1991, calculating the electrical performance of solar cells for five different colors of EVA and found that maximum power output was dramatically decreased when the EVA color altered to a darker brown. Furthermore, Dechthummarong *et al*. [29] compared PV modules before and after 15 years of operation to investigate if the insulation resistance still complied with the IEC 61215 standard [30]. They classified encapsulant discoloration based on four colors: light yellow; yellow; brown; and dark brown. It was found that the modules with light yellow and yellow colors had better electrical performance. Meanwhile modules with brown discoloration were more likely to develop corrosion and delamination failures than modules with yellow discoloration, although insulation resistance when measured in all PV modules was compliant with the IEC standard. Corrosion and more hazardous failures were also found in modules with brown discoloration in a Brazilian study by Diniz *et al.* [31]. Therefore, detecting the early onset of EVA degradation avoids possible hazards through preventative maintenance, such as direct replacement of modules exhibiting signs of early degradation, even if the PV modules are compliant with the IEC standard, while also ensuring the PV modules continue to produce maximal power.

B. Estimation of Encapsulation Degradation

Degradation of encapsulation occurs over time after prolonged exposure, typically years, of the PV module to UV light. Additional stress factors might expedite the degradation process, for example, degradation was observed to commence between 1 and 5 years of deployment in a humid, hot climate [32]. In general, degradation and failures appear in PV encapsulation as discoloration, bubbles, corrosion, and most catastrophically delamination [33], [34]. However, there is not a consensus in the literature as to the time required to reach the failure point as it depends on several stress factors and not only UV exposure. Environmental stresses, such as temperature, hailstorms or sandstorms also contribute to the degradation process [13], [27]. Delamination will lead to a significant reduction in absorbed light, thereby resulting in dramatic reduction of short-circuit current. This, most likely, occurs long after the effects of discoloration have been observed. Corrosion of contacts is typically due to the creation of acetic acid [35], typically occurring long after the effects of discoloration. Corrosion will also cause increased series resistance, but this will not be reflected in changes to the short-circuit current until the series resistance has been increased by a factor of 10 [36]. It has been demonstrated elsewhere [32] that the mean increase in series resistance due to corrosion is a factor of 8.5. Thus, this expected change in series resistance will not significantly affect the model presented in this article. Pern *et al*. [11], demonstrated the difference in transmittance between five different encapsulants, some of which were exposed to natural weathering for more than five years. For analysis, the EVA encapsulants were classified using their evolving color, i.e., from yellow to dark brown, and the difference in their electrical performance when attached to the solar cell was compared. The first encapsulant was non-exposed, the second and the third encapsulants had a yellow-brown color, the fourth had brown color and the fifth had a dark brown color. They also found that in discolored EVA, the reduction of EVA absorption toward longer solar wavelengths did not occur homogeneously

in the PV module, i.e., discoloration of EVA varies from one solar cell to another in a PV module. This forms the basis for the model presented here.

III. Overview of the SPICE Model

SPICE is a long established tool for electrical stimulation of circuits. The adaptation of this simulation tool to modeling solar cells and modules was proposed and developed by Castaner and Silvestre [41]. We have adopted the approach outlined in that book to the specific problem of modeling the effects of reduced optical transmission through the encapsulant. The PSpice model to determine the effects of encapsulant discoloration follows three steps.

1) *Step 1*: Calculation of the transmitted solar spectrum, which is obtained by multiplying the transmittance of the EVA by the AM1.5G solar spectrum.
2) *Step 2*: Simulation of the short-circuit current density, generated from the calculated solar spectrum from step 1.
3) *Step 3*: Using the simulated short-circuit current density obtained in Step 2 to simulate the solar cell's Current-Voltage curve.

The simulation informs the effects of encapsulation degradation on the PV module performance and may be used to identify early onset degradation of the EVA.

A. Standard Solar Spectrum (AM1.5G)

The standard spectrum for PV terrestrial applications is set for air mass 1.5 [37], [38]. Air mass is defined in [39, p.1] as "the path length of the direct solar beam through the atmosphere" and can be calculated as shown in [41, eq. (1)] following formula:

$$\mathrm{AM} = \frac{1}{\cos \vartheta_z} \tag{1}$$

where ϑ_z is the zenith angle. Using SPICE, the standard AM1.5G spectrum was taken from Hulstrom *et al.* [40], and written as a piecewise linear (PWL) source subcircuit by Castaner and Silvestre [41]. In SPICE, the PWL source simplifies the simulation parameters in one source. Thus, changes in any of the source's parameters will be reflected in the simulation results. As mentioned earlier, when optical transmission properties degrade, the PV module will absorb less of the solar spectrum at specific wavelengths. Such a scenario can be simulated by reducing the intensity of some of the wavelengths in the solar spectrum. A greater degradation in the encapsulant will lead to a reduction in the intensity of the transmitted spectrum to the solar cells.

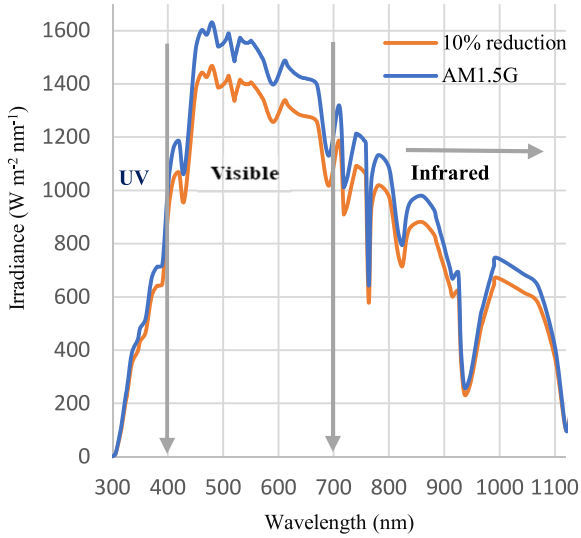

Fig. 1. Simulation of the standard solar spectrum AM1.5G on earth, and standard solar spectrum with a 10% reduction.

Fig. 1 shows the difference between the standard AM1.5G spectrum and the standard spectrum when reduced uniformly by 10% across all wavelengths. The resulting solar irradiance decreases from 994.5 to 895 W m^{-2}, where the total irradiance can be calculated by using numerical integration of the spectrum

$$\int_a^b f(x)\ dx \approx (b-a)\,\frac{\int f(a) + \int f(b)}{2}. \tag{2}$$

B. Short Current Density (J_{sc})

A solar cell is a semiconductor diode with p-type and n-type doped regions that generate electricity from the absorption of light. [41], [42] Depending on the type of semiconductor used, the properties of light reflection and light absorption vary, and they depend on many factors summarized in [41, eq. (3) and eq. (4)]. Indeed, these factors determine the amount of generated photocurrent by the semiconductor and, hence the amount of energy produced [41].

Typically, in a solar cell, the p-type material is identified as the base and the n-type material is called the emitter, and the short-circuit current densities of each are calculated using [41, eq. (3) and eq. (4)] shown at bottom of the next page, where $J_{\mathrm{sc}E}(\lambda)$ is the spectral short-circuit current density at the emitter and $J_{\mathrm{sc}B}(\lambda)$ is the spectral short-circuit current density at the base, both measured in A cm^{-2} nm^{-1}. W_b and W_e are the

$$J_{\mathrm{sc}E}\ (\lambda) = \frac{q\alpha\phi_0\,(1-R)\,L_p}{(\alpha L_p)^2 - 1}\left[-\alpha L_p \mathrm{e}^{-\alpha w_e} + \frac{S_e\frac{L_p}{D_p} + \alpha L_p - \mathrm{e}^{-\alpha W_e}\left(S_e\frac{L_p}{D_p}Ch\frac{W_e}{L_p} + Sh\frac{W_e}{L_p}\right)}{Ch\frac{W_e}{L_p} + S_e\frac{L_p}{D_p}Sh\frac{W_e}{L_p}}\right] \tag{3}$$

$$J_{\mathrm{sc}B}\ (\lambda) = \frac{q\alpha\phi_0^{'}\,(1-R)\,L_n}{(\alpha L_n)^2 - 1}\left[-\alpha L_n - \frac{S_b\frac{L_n}{D_n}\left(Ch\frac{W_b}{L_n} - \mathrm{e}^{-\alpha W_b}\right) + Sh\frac{W_b}{L_n} + \alpha L_n \mathrm{e}^{-\alpha W_b}}{Ch\frac{W_b}{L_n} + S_b\frac{L_n}{D_n}Sh\frac{W_b}{L_n}}\right] \tag{4}$$

thickness of the base and the emitter respectively, both measured in centimetres. R is the reflection coefficient, while α is the absorption coefficient measured in cm^{-1}. ϕ_0 and $\phi_0^{'}$ are the photon spectral flux at the emitter surface and the base-emitter respectively and have units of $\mathrm{photons\ cm}^{-2}\mu\mathrm{m}^{-1}\ \mathrm{s}^{-1}$, $L_n$and L_p are the length of electron and the hole diffusion at the emitter and base layers and both are measured in centimetres. D_n and D_p are the constant diffusion for the base and the emitter respectively, both measured in $\mathrm{cm}^2\ \mathrm{s}^{-1}$. Both S_e and S_b represent the recombination velocity at both sides of the emitter and base and they are also measured in $\mathrm{cm}^2\ \mathrm{s}^{-1}$.

In the simulation the SPICE model was created based on the physical properties of silicon. PSpice version 17.2-2016 and LtSpice version XVII 17.0.0.11, (Analog Devices, USA) were used to run the simulations. To verify the SPICE model for silicon, PC1D software was used. PC1D is a program developed and supported by the University of New South Wales in Australia that numerically determines the photo-response of a silicon solar cell [43]. When the absorption and reflection properties of silicon are calculated, they are then gathered along with the solar spectrum in a SPICE PWL source to accurately simulate the spectral short-circuit current density.

Once light strikes a silicon solar cell, it generates photocurrents at both sides of the diode emitter and base which, when added, determine the total short-circuit current density of the cell. Consequently, the total spectral short-circuits current density is the sum of spectral short-circuit current densities at the emitter and base sides as seen in [41, eq. (5)]

$$J_{\mathrm{sc}\lambda} = J_{\mathrm{sc}E\lambda} + J_{\mathrm{sc}B\lambda}. \tag{5}$$

To find the total short-circuit current density, the sum of spectral short-circuit current densities must be integrated throughout all wavelengths as described in [41, eq. (6)]

$$J_{\mathrm{sc}} = \int_0^{\infty} J_{\mathrm{sc}\lambda}\ \mathrm{d}\lambda = \int_0^{\infty} \left(J_{\mathrm{sc}E\lambda} + J_{\mathrm{sc}B\lambda}\right)\ \mathrm{d}\lambda. \tag{6}$$

C. Current-Voltage I–V of a Solar Cell

By modeling the current density that is generated, this can be then inserted in a PSpice model as a voltage controlled current source (G-device) modified by the incident solar irradiance

$$G_{\mathrm{irrad}} = \frac{J_{\mathrm{sc}}A}{1000}\ .G \tag{7}$$

where G is the incident irradiance in W m^{-2}, and A is the solar cell area in cm^{-2}. The equation uses the standard test condition for PV cells (STC), (AM1.5G spectrum, temperature at 25 °C, and irradiance at 1000 Wm^{-2}).

However, in order to make a realistic model, all other parameters of the solar cell are considered. This is attained by using a PSpice subcircuit to break the solar cell's equivalent circuit into three nodes; the first two nodes are the input nodes that consider the short-circuit current density, the dark current density (J_0), the recombination dark current density (J_{02}), irradiance (G), shunt resistance (R_{sh}), and series resistance (R_s) while the third node is the reference node. The irradiance represents the source that contains the two dark current densities (I_0), and (I_{02}) subtracted from the photogenerated current (I_L) as seen in [41, eq. (8)]

$$I = I_L - I_0\left(e^{\frac{v+IR_s}{\hbar V_T}} - 1\right) - I_{02}\left(e^{\frac{V+IR_s}{2V_T}} - 1\right) - \frac{V+IR_s}{R_{sh}} \tag{8}$$

where V_T is the thermal voltage measured in volts.

To sum up, the model considers all solar cell parameters and encapsulant degradation can be simulated by decreasing the short-circuit current density proportional to the reduction in the optical absorption caused by the encapsulant degradation.

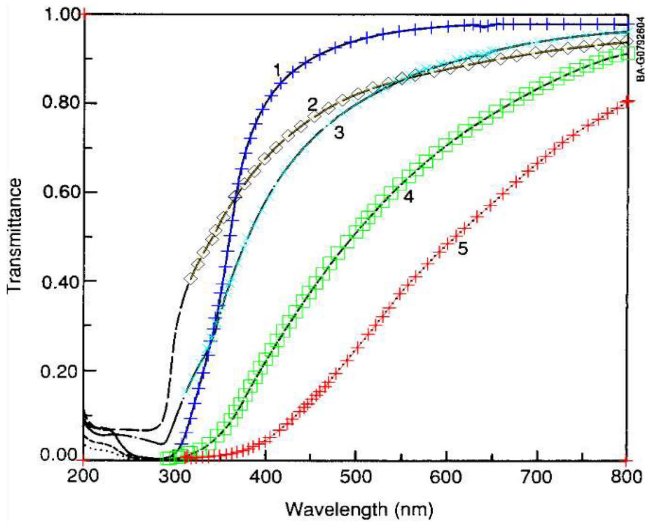

Fig. 2. Transmittance for the five different encapsulants adapted from [9], with extracted transmittance data-points using Engauge Digitizer. Note: extraction below 300 nm was not carried out as these wavelengths are not absorbed by the silicon solar cell.

IV. Simulation of EVA Degradation

A. Transmittance Extraction From Experimental Data

The experimental data used in this simulation study was extracted from Fig. 2 of Pern *et al.* [11]. In their figure, they displayed the transmittance for five degraded EVA encapsulants based on their colors. Samples 1, 4, and 5 were laminated in two glass plates and exposed to an RS4 sun lamp at 90°C for 1600 h. Samples 2 and 3 were taken from weathered PV modules. Extracting the data-points of the five EVA encapsulants was done using the Engauge Digitizer Software Program Version 10.11 as shown in Fig. 2. After obtaining the transmittance for each EVA type, these were then multiplied by the solar spectrum to obtain the modified received spectrum, and hence the expected short-circuit current density J_{sc} for each, as explained in Section IV-B.

However, this experimental data extends only as far as 800 nm with no information about the effective change in transmittance from 800 to 1100 nm. King *et al.* [18] conducted another study where the variation in transmittance between 800 and 1100 appeared less than 1% and thus transmittance changes over this wavelength range are considered negligible in this article. Taking into consideration cases 4 and 5 from Fig. 2, representing a worst

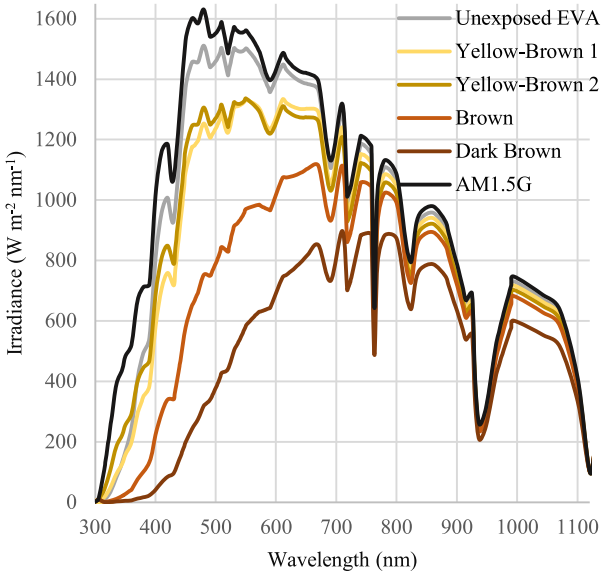

Fig. 3. Six simulated solar spectra demonstrating the degradation of EVA encapsulant expected from Pern *et al.* [11].

case change in transmittance of up to 12% over this wavelength range would result in an output current density increase from 17.98 to 18.4 mA cm^{-2}, representing an error of 2.8%, which is sufficiently small that it is ignored in this article.

In addition, this model considers only a uniform reduction is transmittance across the cell. Further consideration should be given to situations where the discoloration is not uniform, due to photobleaching, for example. This is beyond the scope of the current model.

B. Simulation of Solar Spectrum for the Five Encapsulant Scenarios

After obtaining transmission spectra for the five degradation scenarios of EVA, these were multiplied by the AM1.5G solar spectrum before being used in the simulation. The transmitted solar spectra are shown in Fig. 3.

C. Simulation of the Short-Circuit Current Densities

Using the transmitted solar spectra, the short-circuit current densities J_{sc} for the five degraded encapsulants are calculated. The J_{sc} is found from the wavelength integral of the spectral short current density ($J_{sc\lambda}$). Simulating the $J_{sc\lambda}$ based on the photon wavelength is easily achieved using SPICE, as seen in Fig. 4.

As a result of the $J_{sc\lambda}$ simulations, it is observed from Table I that the value of J_{sc} for the two yellow-brown encapsulants differs only slightly. This is shown in Fig. 4, where the J_{sc} curves for these two cases are overlapping. This shows that even if the transmittance spectra for yellow-brown encapsulants differ, they end up generating nearly the same short-circuit current density.

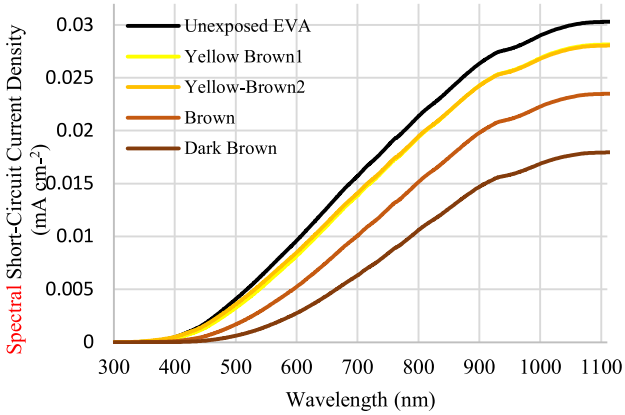

Fig. 4. Simulation of the spectral short-circuit current density for the unexposed and four degraded encapsulant scenarios.

TABLE I
VALUES OF THE SHORT-CIRCUIT CURRENT DENSITY FOR THE FIVE ENCAPSULANT SCENARIOS

Encapsulant Colour	J_{sc} (mA cm^{-2})
Unexposed Encapsulant	30.34
Yellow-Brown-1 Encapsulant	28.09
Yellow-Brown-2 Encapsulant	28.2
Brown Encapsulant	23.53
Dark Brown Encapsulant	17.98

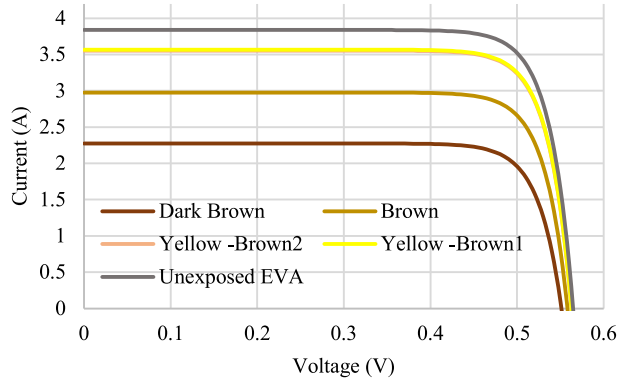

Fig. 5. Simulation of the *I–V* curves for the five encapsulant scenarios.

D. Simulation of the I–V Curves for the Five Degraded Encapsulant Scenarios

After finding the value of short-circuit current density for each degraded encapsulant in a PV solar cell, it is now possible to simulate the *I–V* curves by inserting these values into the SPICE code as explained in Section III-C.

The code considers STC for PV modules by specifying the irradiance to be 1000 W m^{-2}. Fig. 5 shows the generated *I–V* curves for each encapsulant degradation scenario. Once the *I–V* curves are generated, other values of short-circuit current (I_{sc}), open-circuit voltage (V_{oc}), and maximum power output, can be extracted and compared.

TABLE II
VALUE OF *ISC*, *VOC*, AND P_{MAX} FOR THE FIVE ENCAPSULANT DEGRADATION SCENARIOS ALONG WITH A FURTHER 5%, AND 10% REDUCTION IN THE DARK ENCAPSULANT TRANSMITTANCE, AND THEIR RATIO RELATIVE TO THE UNEXPOSED EVA VALUES

Encapsulant Colour	Isc (A)	Ratio to Isc	G (W/m²)	Ratio to G	Voc (mV)	Ratio to Voc	P_{max} (W)	Ratio to P_{max}	Fill Factor
Unexposed Encapsulant	3.84	1.00	942.3	1	565	1	1.78	1	0.818
Yellow-Brown 1	3.57	0.930	885.1	0.939	563	0.996	1.646	0.924	0.819
Yellow-Brown 2	3.55	0.924	879.8	0.934	562	0.995	1.628	0.914	0.816
Brown	2.97	0.776	746.6	0.792	558	0.988	1.363	0.765	0.822
Dark Brown	2.27	0.593	588.4	0.624	550	0.973	1.022	0.574	0.819
Dark Brown - 5%	2.05	0.532	563.9	0.598	549.7	0.973	0.98	0.55	0.825
Dark Brown - 10%	1.94	0.503	544.4	0.577	546.7	0.967	0.865	0.486	0.813

It is worth mentioning that Pern *et al.* [11], had attached the discolored encapsulants onto reference PV solar cells to compare their electrical performance. However, it was not claimed or clarified in their study whether they attached the same encapsulants used to obtain the transmittance measurements in their Fig. 2. Even without this clarification, the SPICE simulation here can still be compared to their results because they stated the difference in P_{max} percentage between clear and colored EVA.

V. RESULTS AND DISCUSSION

A. Correlations Between EVA Transmittance and Electrical Parameters

For the purposes of the simulation the solar cell area was taken as 126.6 cm^2 and J_{sc} was 0.0323 A cm^{-2}. The simulation did not consider the cell parameters used by Pern *et al.* but only considered the optical transmission figure presented in [11]. It is the relative change in P_{max} from the Pern study that match those presented here in this article.

From Table II, it is shown that P_{max} is reduced by more than 50% if the spectrum of the dark brown EVA is further reduced by 10%. The addition of simulated data points for reduced transmittance of 5% and 10% from dark brown have been included to take the cell to a reduction of P_{max} by more than 50% and thereby to a point of failure. The reduction in the absorbed solar spectrum is directly proportional to the reduction in the EVA's transmittance. The short-circuit current, open-circuit voltage, maximum power output and fill factor were compared as a function of transmitted solar irradiance as shown in Fig. 6 . From these results, it is clearly shown that the short-circuit current shows the greatest variation, as expected, as the light transmitted is reduced due to EVA degradation. The open-circuit voltage was only slightly reduced by at most 3.5% in the worst case scenario.

These findings, where I_{sc} changes significantly, and where V_{oc} is only slightly affected, agree, unsurprisingly, with the findings in the experimental results reported by Pern *et al.* [11]. However, the simulation does allow quantification of the rate of reduction in transmitted light with increased EVA degradation and it is this slope that can be used to determine early onset degradation, as will be shown later

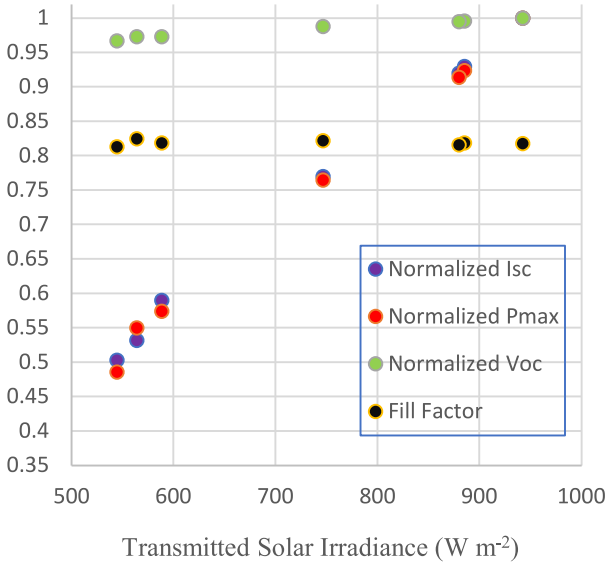

Fig. 6. Relationships between received solar irradiance via encapsulant degradation scenarios and electrical parameters of the solar cell. The short-circuit current, maximum power output, and open-circuit voltage were normalized relative to their value in the unexposed EVA degradation scenarios and electrical parameters of the solar cell.

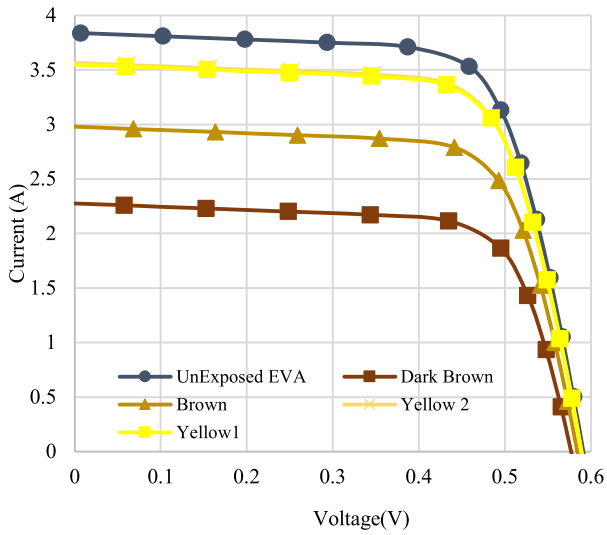

Fig. 7. *I–V* curves generated from a solar cell with five encapsulant scenarios simulated in the PC1D modeling program.

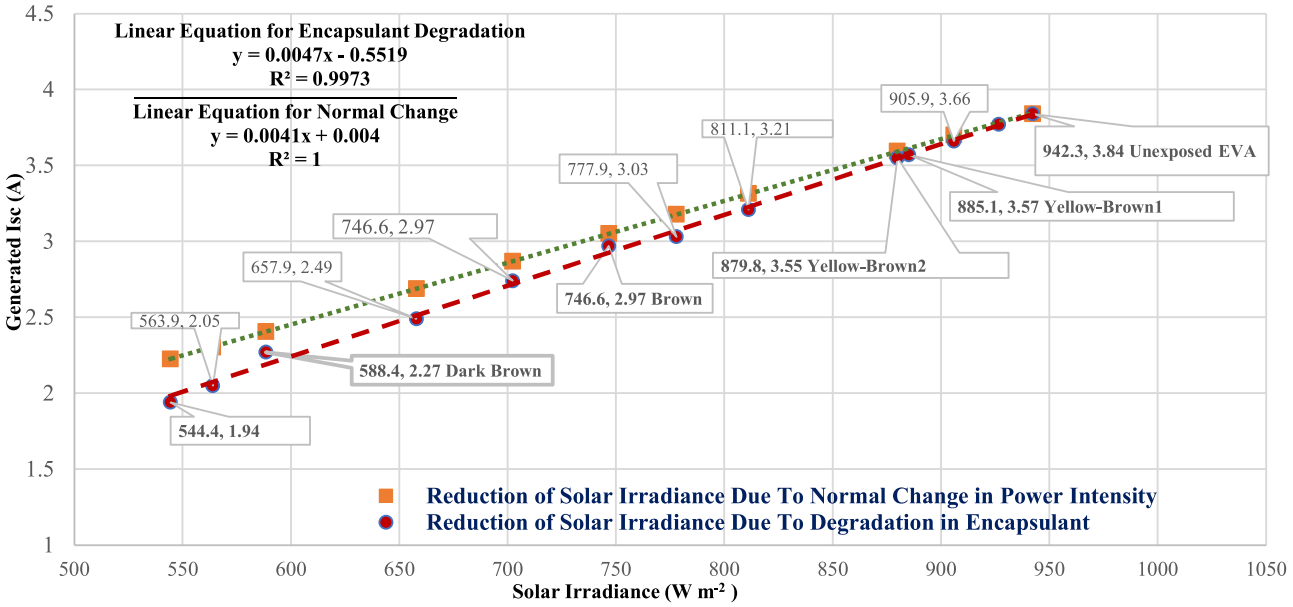

Fig. 8. Linear fit models between the solar irradiance and the generated short-circuit current for EVA degradation Vs normal change of solar irradiance started from the same irradiance EVA received when it was clear. When the $P_{\max}$ falls below 50% of the original power the cell is considered to have failed.

TABLE III
COMPARISON BETWEEN THE GENERATED *I*SC FROM PC1D AND SPICE FOR THE FIVE EVA DEGRADATION SCENARIOS

Encapsulant Degradation Scenario	I_{sc} (A) PC1D	I_{sc} (A) SPICE
Unexposed EVA	3.84	3.84
Yellow-brown 1	3.57	3.57
Yellow -Brown 2	3.55	3.55
Brown	2.97	2.98
Dark Brown	2.27	2.28

B. Simulation Verification Using the PC1D PV Modeling Software

For validation purposes, the encapsulant degradation scenarios were also simulated using the PC1D simulator. Since it was found from the previous section that the variation in short-circuit current is the strongest measurable indicator of the EVA degradation, the comparison is based on the generated I_{sc} values from both the SPICE and the PC1D models. In PC1D, the solar cell used in the simulation was a default cell named PVCEll.PERN. The solar spectra that were simulated for EVA degradation scenarios in SPICE were also used to run the simulations in PC1D. The simulation results from PC1D can be given in Table III and are also demonstrated in Fig. 7. As can be seen from Table III, the generated short-circuit current derived from PC1D corresponds favorably to the values obtained using SPICE.

C. Modeling the Onset of EVA Degradation

Any reduction in the absorbed solar irradiance results in a reduction in the short-circuit current. Where there is a spectrally neutral reduction in solar irradiance, due for example to seasonal variations in intensity, there is a reliably determined value for short-circuit current. In cases where a short-circuit current value is measurably lower than expected from independently measured solar irradiance, the EVA degradation process may have begun. It is noted that I_{sc} is also reduced via other factors such as dust accumulation, corrosion, and delamination. Hence, a single reduction of short-circuit current at a particular solar irradiance cannot be used as a decisive technique for the detection of EVA degradation. From Fig. 6, six data points showing different stages of EVA degradation are plotted, demonstrating a linear relationship between the short-circuit current and transmitted solar irradiance reduced by EVA degradation. This linear relationship provides, through measurement of slope, an accurate technique to determine the onset of EVA degradation in a way that a single measurement of short-circuit current cannot.

In deployed PV plants, instruments that measure electrical parameters and solar irradiance are routinely installed to monitor the system [44], [45]. The measured data is collected and stored as part of the data acquisition system. This can be compared to a linear model relating solar irradiance to measured and expected short-circuit current. The slope of the linear fit can be used as a control model to observe the EVA condition. Routinely, new data is collected for short-circuit current at the same irradiance level, and if the new linear fit shows an increased slope over that expected for normal irradiance changes, it can be determined that the EVA degradation process has begun.

As can be seen from Fig. 8 normal (uniform) reductions in solar irradiance when correlated with the generated I_{sc} have a different slope to the one that demonstrates EVA degradation. Based on this deviation from expected slope the early onset

of EVA degradation can be predicted even before yellowing is observable.

VI. Conclusion

Most commercial solar cell manufacturers continue to use EVA as an encapsulant, despite its vulnerability to UV degradation over the operating life of the cells, resulting in reduced power output and even complete failure of modules. In this article, the published literature on EVA degradation has been reviewed. Most of the studies report results of lab experiments exposing the EVA encapsulant to different stress factors. Some studies had found that EVA degradation starts before the color alters to yellow and becomes more severe once the color changes to brown. This article focused on the simulation of such scenarios based on encapsulant discoloration, and hence optical transmission. Each encapsulant color generates a different I–V curve when attached to a solar cell and delivers a different $P_{\max}$. A novel method has been proposed whereby the slope of the linear relationship between the degree of EVA degradation and in the corresponding short-circuit current is compared to the slope expected in the case of uniformly reduced optical transmission. The application of this model requires the use of monitoring devices to determine the local solar irradiance thereby differentiating between generated $I_{\rm sc}$ and expected $I_{\rm sc}$.

References

[1] S. Chander, A. Purohit, A. Nehra, S. Nehra, and M. Dhaka, "A study on spectral response and external quantum efficiency of mono-crystalline silicon solar cell," *Int. J. Renewable Energy Res.,* vol. 5, no. 1, pp. 41–44, 2015.

[2] C. Peike, I. Hädrich, K.-A. Weiß, and I. Dürr, "Overview of PV module encapsulation materials," *Photovolt. Int.,* vol. 19, pp. 85–92, 2013.

[3] O. Hasan and A. Arif, "Performance and life prediction model for photovoltaic modules: Effect of encapsulant constitutive behavior," *Sol. Energy Mater. Sol. Cells,* vol. 122, pp. 75–87, 2014.

[4] D. C. Miller *et al.*, "Degradation in photovoltaic encapsulant transmittance: Results of the first PVQAT TG5 artificial weathering study," *Prog. Photovolt., Res. Appl.,* vol. 27, no. 5, pp. 391–409, 2019.

[5] M. López-Escalante, L. J. Caballero, F. Martín, M. Gabás, A. Cuevas, and J. Ramos-Barrado, "Polyolefin as PID-resistant encapsulant material in PV modules," *Sol. Energy Mater. Sol. Cells,* vol. 144, pp. 691–699, 2016.

[6] M. Kempe, "Overview of scientific issues involved in selection of polymers for PV applications," in *Proc. 37th IEEE Photovolt. Specialists Conf.*, 2011, pp. 85–90.

[7] J. Kapur, K. M. Stika, C. S. Westphal, J. L. Norwood, and B. Hamzavytehrany, "Prevention of potential-induced degradation with thin ionomer film," *IEEE J. Photovolt.*, vol. 5, no. 1, pp. 219–223, Jan. 2015, doi: 10.1109/JPHOTOV.2014.2365465.

[8] B. M. Habersberger, P. Hacke, and L. S. Madenjian, "Evaluation of the PID-s susceptibility of modules encapsulated in materials of varying resistivity," in *Proc. IEEE 7th World Conf. Photovolt. Energy Convers., Joint Conf. 45th IEEE Photovolt. Specialists, 28th Eur. Photovolt.Solar Energy Conf. Exhib. 34th EU Photovolt. Solar Energy Conf. Exhib.*, 2018, pp. 3807–3809, doi: 10.1109/PVSC.2018.8548117.

[9] C. Peike, L. Purschke, K.-A. Weiss, M. Köhl, and M. Kempe, "Towards the origin of photochemical EVA discoloration," in *Proc. IEEE 39th Photovolt. Specialists Conf.*, 2013, pp. 1579–1584.

[10] A. Badiee, I. Ashcroft, and R. D. Wildman, "The thermo-mechanical degradation of ethylene vinyl acetate used as a solar panel adhesive and encapsulant," *Int. J. Adhesion Adhesives,* vol. 68, pp. 212–218, 2016.

[11] F. Pern, A. Czanderna, K. Emery, and R. Dhere, "Weathering degradation of EVA encapsulant and the effect of its yellowing on solar cell efficiency," in *Proc. Rec. 22nd IEEE Photovolt. Specialists Conf.*, 1991, pp. 557–561.

[12] W. Stark and M. Jaunich, "Investigation of ethylene/vinyl acetate copolymer (EVA) by thermal analysis DSC and DMA," *Polym. Testing,* vol. 30, no. 2, pp. 236–242, 2011.

[13] M. C. C. de Oliveira, A. S. A. D. Cardoso, M. M. Viana, and V. d. F. C. Lins, "The causes and effects of degradation of encapsulant ethylene vinyl acetate copolymer (EVA) in crystalline silicon photovoltaic modules: A review," *Renewable Sustain. Energy Rev.,* vol. 81, pp. 2299–2317, 2018.

[14] J. Frederick, H. Snell, and E. Haywood, "Solar ultraviolet radiation at the earth's surface," *Photochem. Photobiol.,* vol. 50, no. 4, pp. 443–450, 1989.

[15] E. Klampaftis, M. Congiu, N. Robertson, and B. S. Richards, "Luminescent ethylene vinyl acetate encapsulation layers for enhancing the short wavelength spectral response and efficiency of silicon photovoltaic modules," *IEEE J. Photovolt.,* vol. 1, no. 1, pp. 29–36, Jul. 2011.

[16] K. Cristofoli, "Preparação e caracterização de filmes de PEBD aditivados com fotoestabilizantes para a proteção de espumantes rose," M.S. thesis, Dept. Mater, Universidade De Caxias Do Sul, Caxias do Sul, Brazil, 2014. [Online]. Available: https://repositorio.ucs.br/handle/11338/715?locale-attribute=en

[17] W. H. Holley *et al.*, "Investigation into the causes of browning in EVA encapsulated flat plate PV modules," in *Proc. IEEE 1st World Conf. Photovolt. Energy Convers, Joint Conf. Photovolt. Specialists, Eur. Photovolt. Solar Energy Conf. Exhib., PSEC*, 1994, pp. 893–896.

[18] D. King, M. Quintana, J. Kratochvil, D. Ellibee, and B. Hansen, "Photovoltaic module performance and durability following long-term field exposure," *Prog. Photovolt.,Res. Appl.,* vol. 8, no. 2, pp. 241–256, 2000.

[19] D. King, F. Pern, J. Pitts, C. Bingham, and A. Czanderna, "Optical changes in cerium-containing glass as a result of accelerated exposure testing [of PV modules]," in *Proc. Conf. Rec. 26th IEEE Photovolt. Specialists Conf.*, 1997, pp. 1117–1120.

[20] M. D. Kempe, T. Moricone, and M. Kilkenny, "Effects of cerium removal from glass on photovoltaic module performance and stability," in *Reliability of Photovoltaic Cells, Modules, Components, and Systems II*, Bellingham, WA, USA: SPIE, 2009.

[21] S. Jiang, K. Wang, H. Zhang, Y. Ding, and Q. Yu, "Encapsulation of PV modules using ethylene vinyl acetate copolymer as the encapsulant," *Macromol. Reaction Eng.,* vol. 9, no. 5, pp. 522–529, 2015.

[22] P. Arularasu, "Combined UV-temperature-humidity accelerated testing of PV modules: Reliability of UV-cut and UV-pass EVA encapsulants," M.S. thesis, Arizona State Univ., Tempe, AZ, USA, 2019. [Online]. Available: https://core.ac.uk/download/pdf/200249834.pdf

[23] *Plastics - Determination of Yellowness Index and Change in Yellowness Index*, ISO Standard 17223:2014, May 2014. [Online]. Available: https://www.iso.org/obp/ui/#iso:std:iso:17223:ed-1:v1:en

[24] M. C. C. de Oliveira *et al.*, "Comparison and analysis of performance and degradation differences of crystalline-Si photovoltaic modules after 15-years of field operation," *Sol. Energy,* vol. 191, pp. 235–250, 2019.

[25] H. Yong, T. Minemoto, and T. Takahashi, "Dependence of photovoltage on incident photon energies investigated by Photo-assisted kelvin probe force microscopy on Cu (In, Ga) Se_2 solar cells," in *Proc. IEEE 7th World Conf. Photovolt. Energy Convers. Joint Conf. 45th IEEE Photovolt. Specialists, 28th Eur. Photovolt. Solar Energy Conf. Exhib.,34th EU Eur. Photovolt. Solar Energy Conf. Exhib.*, 2018, pp. 1966–1969.

[26] B. Adothu, S. Chattopadhyay, P. Bhatt, P. Hui, F. R. Costa, and S. Mallick, "Early-stage identification of encapsulants photobleaching and discoloration in crystalline silicon photovoltaic module laminates," *Prog. Photovolt., Res. Appl.*, vol. 28, no. 8, pp. 767–778, 2020.

[27] C. Ferrara and D. Philipp, "Why do PV modules fail?," *Energy Procedia,* vol. 15, pp. 379–387, 2012, doi: 10.1016/j.egypro.2012.02.046.

[28] F. Rosillo and M. Alonso-Garcia, "Evaluation of color changes in PV modules using reflectance measurements," *Sol. Energy,* vol. 177, pp. 531–537, 2019.

[29] C. Dechthummarong, B. Wiengmoon, D. Chenvidhya, C. Jivacate, and K. Kirtikara, "Physical deterioration of encapsulation and electrical insulation properties of PV modules after long-term operation in Thailand," *Sol. Energy Mater. Sol. Cells,* vol. 94, no. 9, pp. 1437–1440, 2010.

[30] C. S. T. Photovoltaic, "Modules—Design qualification and type approval," *Int. Electrotech. Commission,* vol. 1215, pp. 2005–2005, 2005.

[31] A. S. A. Diniz *et al.*, "Evaluation of performance losses and degradation of aged crystalline si photovoltaic modules installed in Minas Gerais (Brazil)," in *Renewable Energy and Sustainable Buildings*. New York, NY, USA: Springer, 2020, pp. 29–46.

[32] S. Chattopadhyay *et al.*, "Visual degradation in field-aged crystalline silicon PV modules in India and correlation with electrical degradation," *IEEE J. Photovolt.,* vol. 4, no. 6, pp. 1470–1476, Nov, 2014.

[33] H. M. Walwil, A. Mukhaimer, F. Al-Sulaiman, and S. A. Said, "Comparative studies of encapsulation and glass surface modification impacts on PV performance in a desert climate," *Sol. Energy,* vol. 142, pp. 288–298, 2017.

[34] D. C. Jordan, T. J. Silverman, J. H. Wohlgemuth, S. R. Kurtz, and K. T. VanSant, "Photovoltaic failure and degradation modes," *Prog. Photovolt., Res. Appl.,* vol. 25, no. 4, pp. 318–326, 2017, doi: 10.1002/pip.2866.

[35] A. Gok, D. A. Gordon, M. Wang, R. H. French, and L. S. Bruckman, "Degradation science and pathways in PV systems," in *Durability and Reliability of Polymers and Other Materials in Photovoltaic Modules*, Amsterdam, The Netherlands: Elsevier, 2019, pp. 47–93.

[36] K. L. Kennerud, "Analysis of performance degradation in CDS solar cells," *IEEE Trans. Aerosp. Electron. Syst.*, vol. AES-5, no. 6, pp. 912–917, Nov. 1969, doi: 10.1109/TAES.1969.309966.

[37] *Terrestrial Solar Spectral Irradiance Tables at Air Mass 1.5 For A 37 Deg Tilted Surface*, ASTM Standard E892-87, 1992.

[38] Photovoltaic *Devices – Part 1: Measurement Principles* for *Terrestrial* PV solar *Devices With Reference Spectral Irradiance Data*, IEC 60904-3:2019, Geneva, Switzerland, Sep. 2006.

[39] C. Riordan and R. Hulstron, "What is an air mass 1.5 spectrum?(Solar cell performance calculations)," in *Proc. IEEE Conf. Photovolt. Specialists*, 1990, pp. 1085–1088.

[40] R. Hulstrom, R. Bird, and C. Riordan, "Spectral solar irradiance data sets for selected terrestrial conditions," *Sol. Cells,* vol. 15, no. 4, pp. 365–391, 1985.

[41] L. Castaner and S. Silvestre, *Modelling Photovoltaic Systems Using PSpice*. Chichester, U.K.: Wiley, 2002.

[42] J. Cotter, J. Guo, P. Cousins, M. Abbott, F. Chen, and K. Fisher, "P-type versus n-type silicon wafers: Prospects for high-efficiency commercial silicon solar cells," *IEEE Trans. Electron Devices,* vol. 53, no. 8, pp. 1893–1901, Aug. 2006.

[43] Photovoltaics Special Research Centre, Univ. of New South Wales, Sydney, NSW, Australia, 2003. Accessed: Nov. 12, 2020. [Online]. Available: https://www.engineering.unsw.edu.au/energy-engineering/research/software-data-links/pc1d-software-for-modelling-a-solar-cell

[44] A. M. Krishna, K. P. Rao, M. B. Prakash, and N. Ramchander, "Data acquisition system for performance monitoring of solar photovoltaic (PV) power generation," *Int. J. Eng. Res. Tech.,* vol. 1, no. 7, pp. 1–6, 2012.

[45] H. Rezk, I. Tyukhov, M. Al-Dhaifallah, and A. Tikhonov, "Performance of data acquisition system for monitoring PV system parameters," *Measurement,* vol. 104, pp. 204–211, 2017.